Reovirus infection is regulated by NPC1 and endosomal cholesterol homeostasis

Paula Ortega,[a,b,c,d] Gwen Taylor,[c,d] Rohit K. Jangra,[e,†] Raquel Tenorio,[a] Isabel Fernández de Castro,[a] Bernardo A. Mainou,[f,††] Robert C. Orchard,[g] Craig B. Wilen,[h] Pamela A. Brigleb,[c,i] Jorna Sojati,[c,i] Kartik Chandran,[e] Cristina Risco,[a,*] and Terence S. Dermody,[c,d,i,*]

[a]Cell Structure Laboratory, National Center for Biotechnology, CNB-CSIC, campus UAM, Cantoblanco, 28049 Madrid, Spain

[b]PhD Program in Molecular Biosciences, Autonoma de Madrid University, 28049 Madrid, Spain

[c]Department of Pediatrics, University of Pittsburgh School of Medicine, Pittsburgh, Pennsylvania, USA

[d]Institute of Infection, Inflammation, and Immunity, UPMC Children's Hospital of Pittsburgh, Pittsburgh, Pennsylvania, USA

[e]Department of Microbiology and Immunology, Albert Einstein College of Medicine, Bronx, New York, USA

[f]Department of Pediatrics, Vanderbilt University School of Medicine, Nashville, Tennessee, USA

[g]Department of Immunology, University of Texas Southwestern Medical Center, Dallas, Texas, USA

[h]Departments of Laboratory Medicine and Immunobiology, Yale University School of Medicine, New Haven, Connecticut, USA

[i]Department of Microbiology and Molecular Genetics, University of Pittsburgh School of Medicine, Pittsburgh, Pennsylvania, USA

[†]Current address: Department of Microbiology and Immunology, Louisiana State University Shreveport, Shreveport, Louisiana, USA

[††]Current address: Centers for Disease Control and Prevention, Atlanta, Georgia, USA

[*]Corresponding authors: crisco@cnb.csic.es and terence.dermody@chp.edu

Running title: Reovirus infection is regulated by NPC1 and endosomal cholesterol homeostasis

ABSTRACT Cholesterol homeostasis is required for the replication of many viruses, including Ebola virus, hepatitis C virus, and human immunodeficiency virus-1. Niemann-Pick C1 (NPC1) is an endosomal-lysosomal membrane protein involved in cholesterol trafficking from late endosomes and lysosomes to the endoplasmic reticulum. We identified NPC1 in CRISPR and RNA interference screens as a putative host factor for infection by mammalian orthoreovirus (reovirus). Following internalization via clathrin-mediated endocytosis, the reovirus outer capsid is proteolytically removed, the endosomal membrane is disrupted, and the viral core is released into the cytoplasm where viral transcription, genome replication, and assembly take place. We found that reovirus infection is significantly impaired in cells lacking NPC1, but infection is restored by treatment of cells with hydroxypropyl-β-cyclodextrin, which binds and solubilizes cholesterol. Absence of NPC1 did not dampen infection by infectious subvirion particles, which are reovirus disassembly intermediates that bypass the endocytic pathway for infection of target cells. NPC1 is not required for reovirus attachment to the plasma membrane, internalization into cells, or uncoating within endosomes. Instead, NPC1 is required for delivery of transcriptionally active reovirus core particles into the cytoplasm. These findings suggest that cholesterol homeostasis, ensured by NPC1 transport activity, is required for reovirus penetration into the cytoplasm, pointing to a new function for NPC1 and cholesterol homeostasis in viral infection.

IMPORTANCE Genetic screens are useful strategies to identify host factors required for viral infection. NPC1 was identified in independent CRISPR and RNA interference screens as a putative host factor required for reovirus replication. We discovered that NPC1-mediated cholesterol transport is dispensable for reovirus attachment, internalization, or disassembly but required for penetration of the viral disassembly intermediate from late endosomes into the cytoplasm. These findings pinpoint an essential function for cholesterol in the entry of reovirus and raise the possibility that cholesterol homeostasis regulates the entry of other viruses that penetrate late endosomes to initiate replication.

INTRODUCTION

Viral replication is dependent on cellular proteins and pathways for entry, transport, and release of the viral genome to sites of replication in the cell. Viral attachment to host cells occurs by interactions with cell-surface proteins, lipids, and carbohydrate moieties at the plasma membrane and often triggers virus uptake by receptor-mediated endocytosis (1-7). Viruses that traverse through endosomes must escape the endosomal compartment and release their genomes at sites of replication to initiate productive infection. Enveloped viruses generally accomplish endosomal escape using mechanisms involving receptor- or pH-mediated fusion of the viral envelope and endosomal membrane (6, 8-10). In contrast, nonenveloped viruses penetrate endosomal membranes by establishing small membrane pores or large membrane disruptions (9, 11-13). While both enveloped and nonenveloped viruses depend on conformational changes of viral structural proteins to escape endosomes, mechanisms underlying nonenveloped virus membrane penetration are not well understood (6).

Mammalian orthoreoviruses (reoviruses) are nonenveloped icosahedral viruses that infect a broad range of mammalian hosts. Reovirus infections are usually asymptomatic in humans, but these viruses have been implicated in development of celiac disease (14). Reovirus virions include two protein shells, the outer capsid, composed primarily of μ1-σ3 heterohexamers, and core (15-17). Within the core, 10 segments of double-stranded (ds) RNA are packaged, distributed by size into three large (L), three medium (M), and four small (S) segments (17). Following receptor-mediated endocytosis, the reovirus outer capsid undergoes a series of conformational changes and disassembly events required for release of transcriptionally active cores into the cytoplasm (18, 19).

99 Within late endosomes, acid-dependent cathepsin proteases catalyze proteolysis
100 of the viral outer-capsid protein σ3 and cleavage of the membrane-penetration protein
101 μ1 to δ and φ, resulting in formation of metastable intermediates termed infectious
102 subvirion particles (ISVPs) (20-24). Endosomal lipid composition induces ISVPs to
103 undergo additional conformational changes resulting in exposure of hydrophobic
104 domains of δ, release of pore-forming fragment μ1N, and formation of ISVP*s (25, 26).
105 Release of μ1N during ISVP-to-ISVP* conversion leads to endosomal penetration and
106 release of the viral core into the cytoplasm where infection progresses (27-31).
107 Although some essential viral and host factors required for reovirus penetration of the
108 endosome are known, the process is still not well understood.
109 In this study, we used RNA interference and CRISPR screens to discover that
110 Niemann Pick C1 (NPC1), an endolysosomal transmembrane protein that mediates
111 cholesterol egress from late endosomes for redistribution to cellular membranes (32-
112 34), is required for reovirus infection. We found that genetic ablation of NPC1 in human
113 brain microvascular endothelial cells (HBMECs) diminishes reovirus infection by virions
114 but not by ISVPs, suggesting that NPC1 is required for steps that differ between virions
115 and ISVPs. Treatment of NPC1-null HBMECs with hydroxypropyl-beta-cyclodextrin
116 (HβCD), a macrocycle that binds and solubilizes cholesterol, restored infectivity by
117 reovirus virions, suggesting that endosomal cholesterol homeostasis contributes to
118 efficient reovirus entry. While NPC1 is not required for viral attachment to the plasma
119 membrane, internalization, or uncoating within endosomes, we found that NPC1 is
120 required for efficient release of reovirus cores from endosomes into the cytoplasm.
121 Together, these findings suggest that cholesterol homeostasis, ensured by NPC1
122 cholesterol transport activity, is essential for reovirus cell entry and penetration into the
123 cytoplasm.

124 **RESULTS**

125 **CRISPR/Cas-9 and siRNA screens for host factors required for reovirus**
126 **infection identify NPC1.** To discover host factors required for reovirus infection, we
127 conducted genome-wide CRISPR/Cas-9 and siRNA-based cell-survival screens. The
128 CRISPR/Cas-9 screen was conducted using BV2 mouse microglial cells with the
129 murine Asiago sgRNA library targeting over 20,000 genes. BV2 CRISPR cell libraries
130 were infected with reovirus strains type 1 Lang (T1L) and type 3 Dearing (T3D) and
131 cultured for nine days prior to isolation of genomic DNA (gDNA) from surviving cells and
132 deep sequencing. STARS analysis was conducted to identify enriched CRISPR gRNAs
133 within the surviving cell population (Fig. 1A and Table S1). The siRNA screen was
134 conducted using HeLa S3 cells transfected with the ON-TARGET plus siRNA whole
135 genome library targeting over 18,000 genes (35). Transfected cells were infected with
136 reovirus strain T3SA+ and scored for viability using an ATP-dependent luminescence
137 assay. T3SA+ contains nine genes from T1L and the S1 gene from strain T3C44-MA
138 (36). T3SA+ binds all known reovirus receptors. Robust Z scores (median absolute
139 deviation) were calculated for each sample (Fig. 1B and Table S2).

140 Key genes and pathways essential for reovirus replication were defined by
141 comparing the CRISPR/Cas-9 and siRNA screen lists using STRING-db (Fig. 1C). In
142 the CRISPR/Cas-9 screen, four functional pathways defined by Gene Ontology (GO)
143 terms were common to both T1L and T3D, including sialic acid biosynthesis and
144 metabolism (Fig. 1D). Sialic acid is a reovirus attachment factor, and genes involved in
145 sialic acid biosynthesis and metabolism, including *Slc35a1*, are required for T3SA+
146 replication in BV2 cells (37). These data provide confidence that the target genes
147 identified in the CRISPR/Cas-9 screen represent biologically significant candidates. We
148 also compared KEGG pathways identified in the CRISPR/Cas-9 and siRNA screens to

149 increase the likelihood of significant gene targets. Ribosome and lysosome pathways
150 were the only pathways common to both screens (Fig. 1E). Lysosomal genes include
151 *Ctsl*, *Neu1*, and *Npc1*. *Ctsl* encodes cathepsin L, which is required for cleavage of the
152 reovirus outer capsid to form ISVPs (22). *Neu1* encodes neuraminidase, a lysosomal
153 sialidase that cleaves sialic acid linkages required for reovirus infectivity (38). *Npc1*
154 encodes NPC1, a cholesterol transporter that resides in the limiting membrane of
155 endosomes and lysosomes (33, 34).

156 **Engineering and characterization of HBMECs with CRISPR-targeted Npc1.**
157 Based on the function of NPC1 in cell entry and replication of other viruses (39) and its
158 identification in both our CRISPR and siRNA screens, we evaluated a potential role for
159 NPC1 in reovirus replication. Human brain microvascular endothelial cells (HBMECs)
160 are susceptible to reovirus infection (40) and amenable to CRISPR/Cas-9 gene editing
161 (41). To facilitate these studies, we used CRISPR/Cas-9 gene editing to engineer a
162 clonal HBMEC cell line lacking the *NPC1* gene (KO cells). The NPC1 KO cells were
163 complemented by stable transfection of a functional NPC1 allele (KO+ cells).

164 The newly engineered NPC1 KO and KO+ cell lines were characterized for
165 NPC1 expression and cholesterol distribution relative to wild-type (WT) HBMECs.
166 Expression of NPC1 in WT, KO, and KO+ cells was determined by immunoblotting. As
167 anticipated, NPC1 expression in KO cells was abrogated relative to WT and KO+ cells
168 (Fig. S1A). There was an observable increase in NPC1 expression in KO+ cells
169 compared with WT cells (Fig. S1B), but the difference was not statistically significant. In
170 the absence of functional NPC1, cholesterol reorganizes from a homogeneous
171 distribution to accumulate in endosomal compartments (32, 33). To define the
172 distribution of cholesterol in NPC1-null HBMECs, we used fluorescent filipin III to label
173 cholesterol in fixed cells and imaged cholesterol distribution using fluorescence

174 microscopy (Fig. S1C). As anticipated, cholesterol distribution was homogeneous in WT
175 (Fig. S1C, left) and KO+ cells (Fig. S1C, right). However, cholesterol accumulated
176 around the nucleus in KO cells (Fig. S1C, center) in a pattern consistent with the
177 distribution of endosomes (Fig. S1D), confirming the absence of functional NPC1. Thus,
178 KO cells display the expected phenotype of altered cholesterol distribution when NPC1-
179 dependent cholesterol transport is disrupted. Furthermore, complementing NPC1
180 expression in KO cells restores the normal distribution of cholesterol, demonstrating
181 that the observed phenotype is specific for NPC1 expression.

182 **Reovirus infection by virions but not by ISVPs is impaired in NPC1 KO**
183 **cells.** ISVPs prepared by treatment of virions *in vitro* with intestinal or endosomal
184 proteases bind to reovirus receptors and enter target cells by direct penetration of the
185 plasma membrane and bypass requirements for internalization into the endocytic
186 compartment and acid-dependent proteolysis (21, 22, 42). To determine whether NPC1
187 is required for reovirus replication, and further whether NPC1 mediates a step in the
188 infectious cycle that differs between virions and ISVPs, we adsorbed WT, KO, and KO+
189 cells with reovirus strain T1L M1 P208S virions or ISVPs. Reovirus T1L M1-P208S
190 contains a point mutation in the M1 gene that causes viral factories to have a globular
191 morphology similar to the morphology of factories formed by reovirus T3D (43), which
192 renders infected cells easier to detect. Infected cells were visualized by
193 immunofluorescence (IF) staining for reovirus antigen at 18 h post-adsorption (Fig. 2).
194 Following adsorption with reovirus virions, the number of infected KO cells was reduced
195 by approximately 50% relative to infected WT and KO+ cells (Fig. 2A). A similar
196 reduction in the number of infected KO cells relative to WT and KO+ cells was observed
197 when WT, KO, and KO+ cells were adsorbed with T1L, T3D, and T3SA+ virions, the
198 reovirus strains used in the CRISPR/Cas9 and siRNA screens (Fig. S2). In contrast, no

199 significant differences in numbers of infected cells were observed following adsorption
200 of WT, KO, and KO+ cells with ISVPs (Fig. 2B). Viral progeny production and release
201 was determined by quantifying viral titers in cell lysates and supernatants at 0, 24, and
202 48 h following adsorption of WT, KO, and KO+ cells with virions or ISVPs. Following
203 infection by virions, viral titers in lysates and supernatants of KO cells were 10- to 100-
204 fold less than those in WT and KO+ cells (Fig. 2C and E). In contrast, following infection
205 by ISVPs, viral titers in lysates and supernatants of all three cell types were comparable
206 (Fig. 2D and F). Together, these results suggest that NPC1 is required for reovirus
207 infection and functions at a step in the infectious cycle that differs between virions and
208 ISVPs.

209 **NPC1 is not required for reovirus attachment, internalization, or uncoating.**
210 Reovirus entry can be divided into four main stages: viral binding to cell-surface
211 receptors, viral internalization by endocytosis, proteolytic removal of the viral outer
212 capsid, and penetration of the core from late endosomes into the cytosol (19). We
213 characterized NPC1 KO cells for the capacity to support each step of the reovirus entry
214 pathway to define the function of NPC1 in reovirus infection. To determine whether
215 NPC1 is required for reovirus attachment to target cells we quantified viral binding using
216 flow cytometry. The quantity of virus bound to the surface of all three cell types was
217 comparable, and no statistically significant differences were observed (Fig. 3A). These
218 data suggest that reovirus attachment to cells is not dependent on expression of NPC1.

219 To determine whether NPC1 is required for reovirus to access the endocytic
220 pathway of target cells, WT, KO, and KO+ cells were adsorbed with fluorescently-
221 labeled reovirus particles and monitored for reovirus uptake using live-cell imaging. We
222 found that kinetics of reovirus internalization into WT, KO, and KO+ cells were
223 comparable. High-magnification videos (Videos 1, 2, and 3) along with static images

224 obtained at different intervals (Fig. 3B) demonstrate that attached reovirus particles
225 internalize slowly in the first ~ 0 - 10 min post-adsorption. During this time, reovirus
226 particles remain in the periphery, with a few particles coalescing to form large
227 fluorescent puncta. Convergence of immunofluorescent signals suggests co-transport
228 of multiple viral particles in the same endocytic compartment, similar to that observed
229 during reovirus entry into neurons (44). After ~ 15 min post-adsorption, there was rapid
230 recruitment of almost every fluorescent puncta to the perinuclear region.

231 To more precisely define the movement of reovirus virions during entry, we
232 analyzed the trajectories of individual fluorescent virions in Videos 1, 2, and 3 over 36
233 min using the Spot detector plugin function from Icy software. Trajectory colors change
234 over time in which each color corresponds to an interval of ~ 7.5 min in the time-lapse
235 videos (Videos 4, 5, and 6). Analysis of the time-dependent trajectories confirms
236 observations made in the live-imaging videos. Video-microscopic analysis
237 demonstrates that reovirus virions are internalized rapidly into HBMECs and that virion
238 uptake into the endocytic pathway is not impaired in the absence of NPC1.

239 Following internalization of reovirus virions, acid-dependent cathepsin proteases
240 in late endosomes catalyze disassembly. During disassembly, proteolytic cleavage of
241 the outermost capsid protein, σ3, exposes the membrane-penetration protein, μ1, which
242 is subsequently cleaved to form a variety of intermediates that lead to penetration of the
243 core particle into the cytoplasm (20-24, 27-30). Cells lacking NPC1 have increased
244 endosomal pH and decreased cathepsin activity (45), which could impair reovirus
245 uncoating. To determine whether NPC1 is required for reovirus disassembly, we
246 defined the kinetics of reovirus outer-capsid proteolysis by following the formation of the
247 δ cleavage fragment of the μ1 protein in WT, KO, and KO+ cells. Cells were adsorbed
248 with reovirus virions, and viral proteins in cell lysates were visualized by immunoblotting

249 at 0, 1, 2, and 3 h post-adsorption using a reovirus-specific antiserum. No significant
250 differences in the kinetics of μ1 proteolysis were observed, with an initial δ cleavage
251 product detected 2 h after adsorption in WT, KO, and KO+ cells (Fig. 3C). These data
252 suggest that the cathepsins that catalyze reovirus disassembly are not impaired in
253 NPC1 KO HBMECs. Collectively, these results demonstrate that NPC1 is not required
254 for reovirus receptor binding, internalization, or disassembly.

255 **Escape of reovirus cores from endosomes is impaired in cells lacking**
256 **NPC1.** To determine whether NPC1 is required for escape of reovirus cores into the
257 cytoplasm following disassembly in the endocytic compartment, we imaged cores in
258 fixed cells by IF. Cells were adsorbed with fluorescently labeled reovirus virions and
259 incubated in the presence of cycloheximide for 8 h post-adsorption to inhibit synthesis
260 of new viral proteins and thus ensure detection of proteins from infecting viral particles.
261 Cells were stained with a CD-63-specific antibody to label endosomes and an
262 antiserum specific for reovirus cores and imaged using confocal microscopy. Small
263 puncta consistent with reovirus cores were observed in WT and KO+ cells, while in KO
264 cells, cores appeared to accumulate in larger puncta corresponding to endosomes (Fig.
265 4A). The distribution of virions, cores, and endosomes was determined to quantify the
266 extent of colocalization. The results demonstrate a strong colocalization of cores and
267 endosomes in KO cells (Manders coefficient [Mc]: ~ 0.7), while there was much less
268 colocalization of cores and endosomes in WT and KO+ cells (Mc: ~ 0.3) (Fig. 4B).
269 Colocalization of virions and cores also was more frequent in KO cells (Mc: ~ 0.45) cells
270 than in WT (Mc: ~0.15) or KO+ (Mc: ~0.2) cells, whereas colocalization of virions and
271 endosomes was comparable in all cell types (Mc: ~ 0.6). These data suggest that
272 escape of cores from endosomes is less efficient in the absence of NPC1.

273 To complement the imagining experiments, we quantified newly synthesized viral
274 s4 mRNA using RT-qPCR. WT, KO, and KO+ cells were adsorbed with reovirus, RNA
275 was isolated, and s4 transcripts were quantified at 0, 6, 12, and 24 h post-adsorption.
276 We observed a statistically significant increase in total s4 RNA in WT and KO+ cells at
277 12 and 24 h post-adsorption relative to KO cells (Fig. 5). Together, these results
278 suggest that NPC1 is required for release of transcriptionally active reovirus cores from
279 endosomes into the cytoplasm.

280 **Cholesterol homeostasis is required for reovirus entry.** We thought it
281 possible that NPC1 could serve as an endosomal receptor for reovirus and interact with
282 one or more viral capsid proteins to enable core delivery into the cytoplasm, analogous
283 to the function of NPC1 in Ebola virus infection (46, 47). Alternatively, NPC1 might be
284 required to maintain an endosomal environment with appropriate cholesterol levels to
285 allow cores to penetrate endosomes. To distinguish between these possibilities, we
286 tested whether hydroxypropyl-β-cyclodextrin (HβCD), a cyclic oligosaccharide that
287 triggers cholesterol release from the endo-lysosomal compartment (48, 49) and has
288 shown efficacy in the treatment of the Niemann Pick type C disease (50, 51), for the
289 capacity to overcome the effects of NPC1 deficiency on reovirus infection. To determine
290 whether HβCD treatment redistributes cholesterol from endosomal membranes to a
291 homogeneous distribution in the absence of NPC1, NPC1 KO HBMECs were treated
292 with 1 mM HβCD, a non-toxic concentration (Fig. S3A), or PBS for 48 h prior to staining
293 for the filipin III complex. Cells displaying cholesterol accumulation were distinguished
294 from those with widely distributed cholesterol by quantifying the mean fluorescence
295 intensity (MFI) of filipin III complex staining. Using this approach, an increase in MFI
296 correlates with an increase in cholesterol accumulation. After HβCD treatment, KO cells
297 displayed a significant redistribution of cholesterol, reducing its accumulation in

298 endosomes and enhancing its distribution broadly throughout the cell, correlating with a
299 statistically significant decrease in MFI (Fig. S3B,C). These data demonstrate that
300 HβCD treatment promotes cholesterol efflux in KO cells, resulting in a cholesterol-
301 distribution phenotype comparable to WT and KO+ cells (Fig. S3C).

302 Once we observed that HβCD treatment effectively redistributes cholesterol in
303 KO cells and, thus, functionally complements NPC1 deficiency, we tested whether the
304 reovirus entry defect in KO cells is due to the absence of NPC1 or impaired cholesterol
305 homeostasis. WT, KO, and KO+ cells were pre-treated with 1 mM HβCD or PBS for 24
306 h, adsorbed with reovirus virions or ISVPs, and scored for reovirus infection by
307 immunostaining. Remarkably, HβCD treatment rescued infection of KO cells by reovirus
308 virions (Fig. 6) but did not appreciably affect infection of WT or KO+ cells. HβCD
309 treatment also did not affect infection of WT, KO, or KO+ cells by ISVPs. These data
310 demonstrate that endosomal cholesterol homeostasis regulates reovirus entry by
311 enhancing penetration of the reovirus core particle into the cytoplasm.

312 **DISCUSSION**

313 In this study, we identified NPC1 as a putative host factor required for reovirus infection
314 using genome-wide CRISPR/Cas9 and siRNA-based cell-survival screens. NPC1 is an
315 endolysosomal cholesterol transporter that mediates cholesterol homeostasis (32-34).
316 Disruption of NPC1 results in cholesterol accumulation in late endosomes (Sup. Fig.
317 2C) and leads to Niemann-Pick type C disease (NPCD), an autosomal-recessive
318 neurodegenerative disorder (32). Early steps in reovirus infection, including receptor
319 binding, acid-dependent proteolytic disassembly, and ISVP-to-ISVP* conversion have
320 been well characterized (19). However, penetration of endosomal membranes and
321 release of viral cores into the cytoplasm are poorly understood processes. We used
322 CRISPR/Cas9 gene-targeted HBMECs lacking NPC1 expression to study the function
323 of NPC1 in reovirus infection. We discovered that NPC1 is dispensable for viral binding
324 to cell-surface receptors (Fig. 3A), internalization of viral particles (Fig. 3B), and
325 disassembly of the viral outer capsid (Fig. 3C). However, NPC1 is required for efficient
326 penetration of reovirus cores into the cytoplasm (Fig. 4). Treatment with HβCD reduces
327 cholesterol accumulation in endosomes (Sup. Fig. 3B and 3C) and restores reovirus
328 infectivity in NPC1 KO cells (Fig. 6). These findings suggest that regulation of
329 cholesterol in endosomal compartments is essential for reovirus entry into host cells.

330 NPC1 is required for the replication of several enveloped viruses. The filoviruses
331 Ebola virus and Marburg virus use NPC1 as an intracellular receptor (46, 47). NPC1
332 also functions in enveloped virus replication by maintaining cholesterol homeostasis.
333 Disruption of cholesterol homeostasis by inhibiting NPC1 prevents entry and replication
334 of dengue virus (52) and African swine fever virus (53) and impairs exosome-dependent
335 release of hepatitis C virus (54). Additionally, NPC1 has been implicated in entry of
336 quasi-enveloped forms of hepatitis A virus and hepatitis E virus (55, 56). However,

337 NPC1 had not been previously appreciated to function in the replication of a
338 nonenveloped virus.
339 We found that reovirus binding, internalization, and uncoating do not require
340 NPC1, suggesting that NPC1 does not function as an intracellular receptor for reovirus.
341 Instead, we found that cholesterol accumulation in the endocytic pathway diminishes
342 the efficiency of reovirus core release into the cytoplasm. Using confocal microscopy,
343 we visualized and quantified the distribution of fluoresceinated reovirus virions, reovirus
344 cores, and late endosomes in infected cells (Fig. 4). Reovirus cores accumulate in the
345 lumen of late endosomes in KO cells (Fig. 4A), while virions distribute to endosomes
346 comparably in KO, WT, and KO+ (Fig. 4B). These findings suggest that cores do not
347 escape from endosomes efficiently in the absence of NPC1. RNA synthesis, which
348 occurs in the cytoplasm following release of cores from late endosomes, also was
349 reduced in KO cells relative to WT and KO+ cells (Fig. 5), providing evidence that core
350 escape from endosomes is required for initiation of transcription. It is not apparent how
351 cholesterol accumulation in KO cells blocks core release from late endosomes.
352 In NPCD, disruption of cholesterol homeostasis causes changes in lipid
353 composition of endosomal membranes (57, 58), inverting the ratio of phosphatidyl
354 choline (PC) and phosphatidyl ethanolamine (PE). The change in PC:PE ratio may alter
355 mechanical properties of endosomal membranes by inhibiting intra-endosomal
356 membrane dynamics to favor negative curvature (57, 59). Membrane composition and
357 dynamics can influence viral entry. Negative membrane curvature induced by addition
358 of PE or the action of interferon induced transmembrane protein 3 (IFITM3) impairs
359 adenovirus protein VI-mediated membrane disruption (60) and enveloped virus fusion
360 (61), respectively. Although clearly nonenveloped, reovirus entry also is inhibited by
361 IFITM3 (62). Many nonenveloped viruses use membrane-modifying proteins with the

362 capacity to interact, destabilize, and disrupt membranes to mediate genome release
363 into the cytoplasm (12, 63). However, the role of specific lipids in these processes is not
364 well defined.

365 During reovirus entry, ISVP-to-ISVP* conversion leads to release of
366 myristoylated μ1N, which interacts with late endosomal membranes to facilitate release
367 of cores into the cytoplasm (20-24). PE and PC concentrations in liposomes influence
368 the efficiency of ISVP-to-ISVP* conversion (25). Therefore, it is possible that changes in
369 membrane fluidity, width, or curvature caused by inversion of endosomal membrane
370 PC:PE ratio in NPC1 KO cells impedes membrane insertion of μ1N or formation and
371 expansion of the penetration pore. Additionally, accumulation of cholesterol within the
372 endosomal compartment of NPC1 KO cells could limit recruitment of ISVP*s to
373 membrane-inserted μ1N and the subsequent penetration of reovirus cores. Within the
374 *Reoviridae* family, bluetongue virus (BTV) outer-capsid protein VP5 penetrates late
375 endosomal membranes enriched in phospholipid lysobisphosphatidic acid (LBPA),
376 which is dependent on the anionic charge and membrane fluidic properties of LBPA
377 (64). LBPA enriched late endosomes are also required for efficient rotavirus entry (65).
378 Our data demonstrating the importance of cholesterol homeostasis in reovirus entry
379 along with the role of LBPA in BTV and rotavirus entry suggest that lipid composition of
380 late endosomes influences nonenveloped virus entry and illuminate a potential new
381 target for antiviral therapy.

382 Our findings parallel those of a companion study indicating a function for WD
383 repeat-containing protein 81 (WDR81) in reovirus entry (66). WDR81 was identified in a
384 CRISPR/Cas9 cell-survival screen using mouse embryo fibroblasts and found to be
385 required for a step in reovirus entry that follows ISVP formation. WDR81 is required for
386 the maturation of late endosomes by modulating levels of phosphatidylinositol 3-

387 phosphate (67). These findings, coupled with our studies of NPC1, suggest that ISVPs
388 formed in an altered endocytic compartment of cells lacking either WDR81 or NPC1
389 cannot launch replication, whereas ISVPs adsorbed to the surface of such cells can.
390 We think that alterations in cholesterol distribution might govern this difference in ISVP
391 behavior.

392 Cholesterol accumulation due to NPC1 dysfunction also can lead to alterations in
393 the distribution of host proteins, such as annexin A2 (ANXA2), which was identified in
394 our siRNA screen, and annexin A6 (ANXA6) (68). ANXA2 and ANXA6 are
395 multifunctional proteins involved in endosomal trafficking, segregation of membrane
396 lipids, and membrane curvature regulation through membrane-cytoskeleton
397 rearrangements (69). Disruption of NPC1 leads to increased concentrations of ANXA2
398 and ANXA6 in late endosomes in response to cholesterol accumulation (70, 71). It is
399 possible that cholesterol accumulation in cells lacking NPC1 similarly alters the
400 distribution or function of WDR81. Thus, dysfunction of endosomal proteins in NPC1-
401 null cells might alter potential interactions of μ1N or the reovirus core with specific lipid
402 microdomains or proteins and inhibit core release.

403 Genetic screens are useful approaches to identify host factors required for viral
404 replication and provide valuable information about virus-cell interactions (72, 73).
405 However, genetic screens frequently yield long lists of potential candidates, many of
406 which are false-positives. To increase the likelihood of identifying host factors required
407 for reovirus replication, we compared gene lists obtained from independent genome-
408 wide CRISPR/Cas9 and siRNA-based cell-survival screens. Only 28 genes in the
409 CRISPR/Cas9 screens using strains T1L and T3D were identified in the siRNA screen
410 using strain T3SA+, 19 of which are ribosomal genes (Fig. 1B, C). Of the nine non-
411 ribosomal genes, several encode proteins required for reovirus entry, including those

412 involved in sialic acid biosynthesis and metabolism (*Nans* and *Neu*) (37, 38) and viral
413 disassembly (*Ctsl*) (22).
414 Our findings indicate that NPC1, which was identified in both CRISPR/Cas9 and
415 siRNA screens, is required for efficient release of reovirus cores into the cytoplasm by
416 regulating cholesterol homeostasis. High-resolution studies showing the precise
417 distribution of reovirus virions and cores within endosomes will be required to
418 understand how NPC1 and cholesterol homeostasis regulate core release. These
419 studies will allow us to answer the following new questions: Do cores interact with
420 endosomal membranes in KO cells? Does cholesterol impede interactions of cores with
421 membranes? Are other lipids or proteins required for core release? Our ongoing work to
422 answer these questions will clarify the functional elements of the reovirus entry pathway
423 and lead to new approaches to block the entry of viruses that depend on tightly
424 regulated cholesterol distribution in the endocytic pathway.
425

426

427 **MATERIALS AND METHODS**

428 **Cells and viruses**

429 HBMECs were cultured in growth medium (RPMI 1640 (Gibco) supplemented to
430 contain 10% fetal bovine serum (FBS; VWR 97068-085), 10% Nu Serum (Corning), 1%
431 MEM-vitamins (Corning), 1% sodium pyruvate (Gibco), 1% MEM non-essential amino
432 acids (Gibco), 1% L-glutamine (Gibco), 1% penicillin/streptomycin (Gibco), and 0.1%
433 amphotericin B (Sigma)) or infection medium (growth medium containing 2% FBS). BV2
434 mouse microglial cells were cultured in BV2 maintenance medium (DMEM
435 supplemented to contain 10% FBS, 1% penicillin/streptomycin, 1% sodium pyruvate,
436 and 1% sodium bicarbonate) or selection medium (maintenance media supplemented
437 with 4 μg/ml blasticidin (Thermo Fisher) and 2.5 μg/ml puromycin (Sigma-Aldrich)).
438 HeLa cells were cultured in Dulbecco modified Eagle medium (Gibco) supplemented to
439 contain 10% FBS, minimal essential medium nonessential amino acid solution (Gibco),
440 0.11 mg/mL of sodium pyruvate (Gibco), and 1% penicillin/ streptomycin, and 0.1%
441 amphotericin B (Sigma). Spinner-adapted L929 cells (originally obtained from the
442 Bernard Fields laboratory; ATCC CCL-1) were grown in either suspension or
443 monolayers in Joklik's modified Eagle's minimal essential medium (US Biological;
444 M3867) supplemented to contain 5% FBS, 2 mM L-glutamine, 100 units/ml penicillin,
445 100 μg/ml streptomycin, and 0.1% amphotericin B.

446 Reovirus strains T1L, T3D, T3SA+, and T1L M1-P208S, were prepared from
447 laboratory stocks by plaque purification followed by 3 to 4 passages in L929 cells.
448 T3SA+ contains nine genes from T1L and the S1 gene from T3C44-MA (36). T1L M1-
449 P208S contains a point mutation in the M1 gene that causes viral factories to have a
450 globular morphology similar to the morphology of factories formed by reovirus T3D (43)

451 and can be readily scored for infection. Virions were purified from infected L929 cell
452 lysates using cesium chloride gradient centrifugation as described (74). Viral titers were
453 determined by plaque assay using L929 cells (75) and expressed as plaque forming
454 units per ml (PFU/ml). Reovirus particle concentration was estimated by spectral
455 absorbance of purified virions at 260 nm (optical density at 260 nm [OD_{260}] of 1 =
456 2.1×10^{12} particles/ml) (76).

457 Fluorescent reovirus particles were prepared by diluting 6×10^{12} reovirus
458 particles/ml in 50 mM sodium bicarbonate buffer and incubating with 20 μM Alexa
459 Fluor™ 647 NHS Ester (Succinimidyl Ester) (Invitrogen, A37573) at room temperature
460 (RT) for 90 min, protected from light (77). Labeled virions were dialyzed at 4°C
461 overnight with 2-3 buffer exchanges to remove unreacted dye.

462 ISVPs were prepared by incubating 2×10^{12} purified reovirus particles with 200
463 μg/mL chymotrypsin (Sigma, C3142) at 37°C for 60 min (23). Digestion was terminated
464 by the addition of PMSF to a final concentration of 2 mM. Virion-to-ISVP conversion
465 was confirmed by SDS-PAGE and colloidal blue staining to assess the loss of σ3 and
466 cleavage of μ1C to δ.

467

468 **Antibodies and dyes**

469 Primary antibodies used for indirect immunofluorescence include anti-CD63 (1:250)
470 (Thermofisher, #10628D), reovirus-specific polyclonal rabbit antiserum (1:1000) (78),
471 and T1L core-specific rabbit antiserum (1:250) provided by Max Nibert (79). Alexa Fluor
472 conjugated secondary antibodies (Thermo Fisher, #A11034, #A11030) were used to
473 visualize antigen. Nuclei were stained with 4′,6-diamidino-2-phenylindole (DAPI,
474 Invitrogen, D3571). Primary antibodies used for immunoblotting include reovirus-
475 specific polyclonal rabbit antiserum, NPC1-specific polyclonal rabbit antiserum (Abcam,

476 134113), and mouse GAPDH monoclonal antibody for protein loading controls (Sigma,
477 G8795). Anti-mouse IRDye680RD and anti-rabbit IRDye800CW (Licor) secondary
478 antibodies were used.
479
480 **CRISPR Screen**
481 The screen was conducted and transduction validated as described (80). BV2 cells
482 were transduced with pXPR_101 lentivirus encoding Cas9 (Addgene; 52962) and
483 propagated for 11 days with BV2 Maintenance Medium supplemented to contain
484 blasticidin. These parental BV2 or BV2-Cas9 cells were transduced for 2 days with
485 pXPR_011 expressing eGFP (Addgene; 59702) and a short guide RNA (sgRNA)
486 targeting eGFP at a multiplicity of infection (MOI) of less than 1 PFU/cell. Cells were
487 selected for 5 days with BV2 selection medium. The frequency of eGFP-expressing
488 cells was quantified by flow cytometry.
489 The murine Asiago sgRNA CRISPR library contains six independent genome-
490 wide pools, in which each pool contains unique sgRNAs targeting 20,077 mouse genes.
491 Four pools of the Asiago library were transduced into 5×10^7 BV2 cells at an MOI of 0.2
492 PFU/cell to establish four BV2 libraries. Two days post-transduction, cells were
493 transferred to BV2 Selection Medium and propagated for 5 additional days. For each
494 experimental condition, 10^7 BV2 library cells expressing Cas9 and sgRNAs were
495 seeded in duplicate into T175 tissue culture flasks (Greiner Bio-One). Cells were
496 inoculated with Opti-MEM supplemented to contain PBS (mock) or reovirus strains T1L
497 or T3D at an MOI of 100 PFU/cell. Cells were incubated at RT for 1 h, followed by the
498 addition of 20 mL of DMEM supplemented to contain 10% FBS, 1%
499 penicillin/streptomycin, 1% sodium pyruvate, and 1% sodium bicarbonate. After 2 days
500 post-inoculation (dpi) (mock) or 9 dpi (T1L or T3D conditions), cells were harvested and

501 genomic DNA (gDNA) was isolated from surviving cells using a QIAmp DNA Mini Kit
502 (QIAGEN) according to the manufacturer's instructions.
503
504 **CRISPR screen sequencing and analysis**
505 Illumina sequencing and STARS analyses were conducted as described (81). The
506 gDNA was aliquoted into a 96-well plate (Greiner Bio-One) with up to 10 µg gDNA in 50
507 µL of total volume per well. A polymerase chain reaction (PCR) master mix containing
508 ExTaq DNA polymerase (Clontech), ExTaq buffer (Clontech), dNTPs, P5 stagger
509 primer, and water was prepared. PCR master mix (40 µL) and 10 µL of a barcoded
510 primer were added to each well containing gDNA. Samples were amplified using the
511 following protocol: 95°C for 1 min, followed by 28 cycles of 94°C for 50 s, 52.5°C for 30
512 s, and 72°C for 30 s, and ending with a final 72°C extension for 10 min. PCR product
513 was purified using Agencourt AMPure XP SPRI beads (Beckman Coulter) according to
514 the manufacturer's instructions. Samples were sequenced using a HiSeq 2000
515 (Illumina). Following deconvolution of the barcodes in the P7 primer, sgRNA sequences
516 were mapped to a reference file of sgRNAs from the Asiago library. To account for the
517 varying number of reads per condition, read counts per sgRNA were normalized to 10^7
518 total reads per sample. Normalized values were then log-2 transformed. sgRNAs that
519 were not detected were arbitrarily assigned a read count of 1. sgRNA frequencies were
520 analyzed using STARS software to produce a rank ordered score for each gene. This
521 score correlated with the sgRNA candidates that were above 10% of the total
522 sequenced sgRNAs. Genes scoring above this threshold in either of the two
523 independent subpools and in at least two of the four independent genome-wide pools
524 were assigned a STAR score. In addition to the STAR score, screen results were

525 compared using false discovery rate (FDR) analyses to monitor gene-specific signal
526 versus background noise. Statistical values of independent replicates were averaged.
527
528 **Whole genome siRNA screen and analysis**
529 The whole genome siRNA screen was conducted as described (35) using HeLa S3
530 cells and the Dharmacon ON-TARGETplus® SMARTpool® human siRNA library
531 (Thermo Scientific) and strain T3SA+.
532
533 **Production of NPC1 KO and KO+ cell lines**
534 HBMEC single-cell clones with ablation of the *NPC1* gene were engineered using
535 CRISPR/Cas9-mediated gene editing as described (82) using an NPC1-specific gRNA
536 (5′ GGCCTTGTCATTACTTGAGGGGG 3′, targeting nucleotides 768-790 of the human
537 NPC1 mRNA). Single-cell clones were screened for the loss of NPC1 function by filipin
538 III staining (82). Genotype of the selected NPC1 KO clones was confirmed by Sanger
539 sequencing followed by amplification of the genomic DNA sequences flanking the
540 gRNA target site using forward (5′ TCATAAACACACCAAACTTGGAATC 3′) and
541 reverse (5′ TCCTGCGGCAGAGGTTTTC 3′) primers. Sequences of the NPC1 alleles
542 were deconvoluted using CRISP-ID (83). To confirm the specificity of *Npc1* knockout,
543 cells of a single clone were transduced with a retrovirus vector (pBabe-Puro)
544 expressing human NPC1 as described (47).
545
546 **Indirect immunofluorescence staining**
547 Cells were fixed with 4% paraformaldehyde (PFA, Electron Microscopy Sciences,
548 15712-s) in $PBS^{-/-}$ at RT for 20 min, washed three times with $PBS^{-/-}$, and permeabilized
549 and blocked with 0.1% Triton X-100 and 2% FBS in $PBS^{-/-}$ at RT for 20 min. Cells were

550 incubated sequentially with primary antibody, Alexa Fluor-conjugated secondary
551 antibody, and DAPI diluted in $PBS^{-/-}$ containing 0.1% Triton X-100 and 2% FBS at RT
552 for 30 to 60 min. For cholesterol labeling, fixed and permeabilized cells were incubated
553 with 50 µg/ml filipin III (Sigma, SAE0088) diluted in $PBS^{-/-}$ for 30 min. Coverslips were
554 mounted using Prolong-gold (Molecular Probes). Confocal images were captured using
555 a Leica-SP8 laser scanning confocal microscope equipped with an HCX PL APO
556 63X/1.4 N.A oil objective and processed using Fiji/ImageJ software.
557
558 **SDS-PAGE and Immunoblotting**
559 Cells harvested for protein extraction were lysed in Radioimmunoprecipitation Assay
560 buffer (*RIPA buffer*; Thermo Fisher) supplemented with 1X protease inhibitors (Thermo
561 Fisher). Protein concentration was quantified by Bradford assay (Bio-Rad) following the
562 manufacturer's protocol. Samples for SDS-PAGE were diluted in 5X Laemmli sample
563 buffer (Bio-Rad) containing 10% β-mercaptoethanol and incubated at 95°C for 10 min.
564 Samples for detection of NPC1 were incubated at 70°C for 10 min to prevent
565 aggregation. Equal amounts of protein were electrophoresed in 10% or 4-20% Mini-
566 Protean TGX gels (Bio-Rad). Following electrophoresis, proteins were transferred to
567 nitrocellulose membranes (Bio-Rad) for immunoblotting. Nitrocellulose membranes
568 were incubated with 5% nonfat milk in TBS (50 mM Tris-HCl, pH 7.6; 150 mM NaCl)
569 with 0.1% Tween 20 (TBS-T) and sequentially incubated with primary and secondary
570 antibodies diluted in TBS-T at RT for 1 h. Immunoblot images were captured using an
571 Odyssey CLx imaging system (Li-Cor) and protein bands were quantified using the
572 Image Studio Lite software. Protein expression levels were normalized to GAPDH
573 loading controls.
574

575 **Quantification of reovirus infectivity**

576 In experiments comparing infectivity of reovirus in KO, KO+, and WT HBMECs, cells
577 were adsorbed with 10,000 reovirus virions or 100 ISVPs diluted in Opti-MEM
578 (Invitrogen) at 37°C for 1 h. Following adsorption, the inoculum was removed, and cells
579 were incubated in infection medium for 18 h before fixing in ice-cold methanol. In
580 experiments comparing reovirus infectivity in the presence or absence of HβCD, cells
581 were treated with 1 mM HβCD or PBS for 24 h prior to adsorption with reovirus.
582 Following adsorption, fresh 1 mM HβCD was added to the medium for 18 h before fixing
583 in ice-cold methanol. Fixed cells were washed with $PBS^{-/-}$, blocked with 1% bovine
584 serum albumin (BSA), and incubated sequentially with reovirus-specific polyclonal
585 rabbit antiserum, Alexa Fluor 488-conjugated anti-rabbit antibody, and DAPI in $PBS^{-/-}$
586 containing 0.5% Triton X-100. Cells were imaged using a Lionheart FX automated
587 imager (BioTek) equipped with a 20X air objective, taking four fields-of-view from
588 duplicate samples. Images were processed and signals quantified using Gen5+
589 software (BioTek).

590

591 **Viral binding**

592 KO, KO+, and WT HBMECs were detached from tissue-culture plates using
593 CellStripper dissociation reagent (Corning), quenched with HBMEC medium, and
594 washed with $PBS^{-/-}$. Cells were resuspended in $PBS^{-/-}$ at 10^6 cells/ml and adsorbed with
595 10,000 Alexa Fluor 647-labeled reovirus virions/cell at 4°C for 1 h with agitation. After
596 binding, cells were washed twice with $PBS^{-/-}$ and fixed with 1% paraformaldehyde (PFA)
597 supplemented with propidium iodide to determine cell viability. Cells were analyzed
598 using an LSRII flow cytometer (BD Bioscience). Results were quantified using FlowJo
599 V10 software.

600

601 **Live microscopy of reovirus internalization**

602 KO, KO+, and WT HBMECs were plated on glass-bottom p35 plates and adsorbed with
603 10,000 Alexa 647-labeled reovirus virions/cell at 4°C for 45 min to synchronize
604 infection. The inoculum was removed and replaced with fresh Opti-MEM without
605 phenol-red medium supplemented with 2% FBS. Reovirus transport was imaged using
606 a Leica DMI6000B fluorescence microscope with an HCX PL APO 63X/1.30 Gly
607 objective. Fluorescence and brightfield images were collected from 0 to 40 min post
608 adsorption every ~ 25 sec.

609

610 **Tracking of reovirus transport**

611 Automated tracking of fluorescent reovirus particles in time-lapse images was
612 conducted using Icy bioimage analysis software. Regions of interest (ROI)
613 corresponding to the cell periphery were selected for tracking analysis using the Spot
614 Detector plugin (84). The scale of the object (reovirus cores) to be analyzed was set at
615 a size of ~7 pixels per spot, and the threshold sensitivity was set at 100. Parameters
616 describing transport dynamics were considered as both diffusive and directed for
617 running tracking analysis. Results are presented in colored time-dependent tracks.

618

619 **Quantification of reovirus cores**

620 KO, KO+, and WT HBMECs were adsorbed with 10,000 Alexa Fluor 647-labeled
621 reovirus virions at 37°C for 45 min. The inoculum was removed, and the cells were
622 incubated in infection medium containing 100 µg/ml of cycloheximide for 8 h. After
623 fixation, cells were permeabilized and stained with T1L core-specific rabbit polyclonal
624 serum and anti-CD63 antibody. Confocal images were captured using a Leica-SP8

625 laser scanning confocal microscope equipped with an HCX PL APO 63X/1.4 N.A oil
626 objective and processed using Fiji/ImageJ software. Colocalization of fluorescent
627 reovirus virions (cyan puncta), reovirus cores (green puncta), and late endosomes (red
628 puncta) was analyzed to differentiate infecting virions from cores released into the
629 cytoplasm.
630

631 **RNA extraction and purification**

632 Cells were lysed using TRIzol reagent (Invitrogen). RNA was extracted with chloroform
633 and purified using a PureLink RNA minikit (Invitrogen) with DNase treatment according
634 to the manufacturer's instructions.
635

636 **S4 quantitative RT-PCR**

637 Total S4 RNA was quantified using qScript XLT one-step RT-qPCR ToughMix, Low
638 ROX (Quanta Bioscience) and T3D_S4_qPCR primers (Forward:
639 GAAGCATTTGCCTCACCATAG, Reverse: GATCTGTCCAACTTGAGTGTATTG)
640 according to the manufacturer's instructions. The following RT-qPCR cycling protocol
641 was used: cDNA synthesis (50°C for 10 min), initial denaturation (95°C for 1 min), and
642 40 PCR cycles (95°C for 10 s followed by a data collection step at 60°C for 1 min). S4
643 cDNA was detected using a fluorogenic probe (5′-FAM [fluorescent fluorescein]-
644 AGCGCGCAAGAGGGATGGGA-BHQ [black hole quencher]-1-3′; Biosearch
645 Technologies).
646

647 **Statistical analysis**

648 All data were analyzed using Graphpad Prism 8. Figure legends specify the number of
649 experimental repeats and the statistical test applied for each analysis. Differences were
650 considered statistically significant when *P* values were less than 0.05.

651 **ACKNOWLEDGEMENTS**

652 We thank members of the Dermody and Risco laboratories for many useful discussions.
653 We are grateful to the UPMC Children's Hospital of Pittsburgh Rangos Research
654 Center Cell Imaging Core Laboratory for assistance with microscopy. Special thanks to
655 Dr. Martin Sachse for expert advice and for critical review of the manuscript and to Drs.
656 Sylvia Gutiérrez-Erlandsson and Ana Oña for assistance with confocal microscopy.

657 This work was supported in part by Public Health Service award R01 AI032539
658 (C.R. and T.S.D.) and the Heinz Endowments (T.S.D.) and grants BIO2015-68758-R
659 and RTI2018-094445-B-100 from the Ministry of Science and Innovation of Spain
660 (C.R.).

661

662 **AUTHOR CONTRIBUTIONS**

663 **Conceived and designed experiments**: POG, GT CR TSD. **Performed experiments**:
664 POG GT RKJ BAM RCO CBW. **Analyzed data**: POG GT. **Contributed**
665 **reagents/materials/analysis tools**: RKJ RCO CBW KC HWV. **Wrote original draft**:
666 POG, GT TSD. **Reviewed and edited paper**: POG GT RKJ RT IF BAM RCO CBW
667 PAB JS KC HWV CR TSD.

668

669 **REFERENCES**

670 1. Mercer J, Helenius A. Virus entry by macropinocytosis. Nat Cell Biol.
671 2009;11(5):510-20.

672 2. Mercer J, Schelhaas M, Helenius A. Virus entry by endocytosis. Annu Rev
673 Biochem. 2010;79:803-33.

674 3. Yamauchi Y, Helenius A. Virus entry at a glance. J Cell Sci. 2013;126(Pt
675 6):1289-95.

676 4. Smith AE, Helenius A. How viruses enter animal cells. Science.
677 2004;304(5668):237-42.

678 5. Tsai B. Penetration of nonenveloped viruses into the cytoplasm. Annual review of
679 cell and developmental biology. 2007;23:23-43.

680 6. Staring J, Raaben M, Brummelkamp TR. Viral escape from endosomes and host
681 detection at a glance. J Cell Sci. 2018;131(15).

682 7. Harrison SC. Viral membrane fusion. Virology. 2015;479-480:498-507.

683 8. White JM, Whittaker GR. Fusion of Enveloped Viruses in Endosomes. Traffic.
684 2016;17(6):593-614.

685 9. Sieczkarski SB, Whittaker GR. Viral entry. Current topics in microbiology and
686 immunology. 2005;285:1-23.

687 10. Plemper RK. Cell entry of enveloped viruses. Current opinion in virology.
688 2011;1(2):92-100.

689 11. Stewart PL, Dermody TS, Nemerow GR. Structural basis of nonenveloped virus
690 cell entry. Advances in protein chemistry. 2003;64:455-91.

691 12. Kumar CS, Dey D, Ghosh S, Banerjee M. Breach: Host Membrane Penetration
692 and Entry by Nonenveloped Viruses. Trends Microbiol. 2018;26(6):525-37.

693 13. Banerjee M, Johnson JE. Activation, exposure and penetration of virally
694 encoded, membrane-active polypeptides during non-enveloped virus entry. Curr Protein
695 Pept Sci. 2008;9(1):16-27.

696 14. Bouziat R, Hinterleitner R, Brown JJ, Stencel-Baerenwald JE, Ikizler M, Mayassi
697 T, et al. Reovirus infection triggers inflammatory responses to dietary antigens and
698 development of celiac disease. Science. 2017;356(6333):44-50.

699 15. Dryden KA, Wang G, Yeager M, Nibert ML, Coombs KM, Furlong DB, et al. Early
700 steps in reovirus infection are associated with dramatic changes in supramolecular
701 structure and protein conformation: analysis of virions and subviral particles by
702 cryoelectron microscopy and image reconstruction. J Cell Biol. 1993;122(5):1023-41.

703 16. Zhang X, Ji Y, Zhang L, Harrison SC, Marinescu DC, Nibert ML, et al. Features
704 of reovirus outer capsid protein m1 revealed by electron cryomicroscopy and image
705 reconstruction of the virion at 7.0 Å resolution. Structure. 2005;13(10):1545-57.

706 17. Dermody TS, Parker JS, Sherry B. Orthoreoviruses. In: Knipe DM, Howley PM,
707 editors. Fields Virology. 2. 6th ed. Philadelphia: Lippincott Williams & Wilkins; 2013. p.
708 1304-46.

709 18. Gummersheimer SL, Snyder AJ, Danthi P. Control of capsid transformations
710 during reovirus entry. Viruses. 2021;13(2):153.

711 19. Roth AN, Aravamudhan P, Fernández de Castro I, Tenorio R, Risco C, Dermody
712 TS. Ins and outs of reovirus: vesicular trafficking in viral entry and egress. Trends
713 Microbiol. 2021;29(4):363-75.

714 20. Borsa J, Sargent MD, Lievaart PA, Copps TP. Reovirus: evidence for a second
715 step in the intracellular uncoating and transcriptase activation process. Virology.
716 1981;111(1):191-200.

717 21. Sturzenbecker LJ, Nibert ML, Furlong DB, Fields BN. Intracellular digestion of
718 reovirus particles requires a low pH and is an essential step in the viral infectious cycle.
719 J Virol 1987;61(8):2351-61.

720 22. Ebert DH, Deussing J, Peters C, Dermody TS. Cathepsin L and cathepsin B
721 mediate reovirus disassembly in murine fibroblast cells. J Biol Chem.
722 2002;277(27):24609-17.

723 23. Baer GS, Dermody TS. Mutations in reovirus outer-capsid protein s3 selected
724 during persistent infections of L cells confer resistance to protease inhibitor E64. J Virol.
725 1997;71:4921-8.

726 24. Silverstein SC, Astell C, Levin DH, Schonberg M, Acs G. The mechanism of
727 reovirus uncoating and gene activation in vivo. Virology. 1972;47(3):797-806.

728 25. Snyder AJ, Danthi P. Lipid membranes facilitate conformational changes
729 required for reovirus cell entry. J Virol. 2015;90(5):2628-38.

730 26. Snyder AJ, Danthi P. Lipids cooperate with the reovirus membrane penetration
731 peptide to facilitate particle uncoating. J Biol Chem. 2016;291(52):26773-85.

732 27. Odegard AL, Chandran K, Zhang X, Parker JS, Baker TS, Nibert ML. Putative
733 autocleavage of outer capsid protein m1, allowing release of myristoylated peptide m1N
734 during particle uncoating, is critical for cell entry by reovirus. J Virol. 2004;78(16):8732-
735 45.

736 28. Agosto MA, Ivanovic T, Nibert ML. Mammalian reovirus, a nonfusogenic
737 nonenveloped virus, forms size-selective pores in a model membrane. Proc Natl Acad
738 Sci U S A. 2006;103(44):16496-501.

739 29. Ivanovic T, Agosto MA, Zhang L, Chandran K, Harrison SC, Nibert ML. Peptides
740 released from reovirus outer capsid form membrane pores that recruit virus particles.
741 EMBO J. 2008;27(8):1289-98.

742 30. Chandran K, Farsetta DL, Nibert ML. Strategy for nonenveloped virus entry: a
743 hydrophobic conformer of the reovirus membrane penetration protein m1 mediates
744 membrane disruption. J Virol. 2002;76(19):9920-33.

745 31. Zhang L, Agosto MA, Ivanovic T, King DS, Nibert ML, Harrison SC.
746 Requirements for the formation of membrane pores by the reovirus myristoylated
747 micro1N peptide. J Virol. 2009;83(14):7004-14.

748 32. Carstea ED, Morris JA, Coleman KG, Loftus SK, Zhang D, Cummings C, et al.
749 Niemann-Pick C1 disease gene: homology to mediators of cholesterol homeostasis.
750 Science. 1997;277(5323):228-31.

751 33. Ioannou YA. The structure and function of the Niemann-Pick C1 protein.
752 Molecular genetics and metabolism. 2000;71(1-2):175-81.

753 34. Kwon HJ, Abi-Mosleh L, Wang ML, Deisenhofer J, Goldstein JL, Brown MS, et
754 al. Structure of N-terminal domain of NPC1 reveals distinct subdomains for binding and
755 transfer of cholesterol. Cell. 2009;137(7):1213-24.

756 35. Konopka-Anstadt JL, Mainou BA, Sutherland DM, Sekine Y, Strittmatter SM,
757 Dermody TS. The Nogo receptor NgR1 mediates infection by mammalian reovirus. Cell
758 Host Microbe. 2014;15(6):681-91.

759 36. Barton ES, Connolly JL, Forrest JC, Chappell JD, Dermody TS. Utilization of
760 sialic acid as a coreceptor enhances reovirus attachment by multistep adhesion
761 strengthening. J Biol Chem. 2001;276(3):2200-11.

762 37. Urbanek K, Sutherland DM, Orchard RC, Wilen CB, Knowlton JJ, Aravamudhan
763 P, et al. Cytidine monophosphate N-acetylneuraminic acid synthetase and solute carrier
764 family 35 member A1 are required for reovirus binding and infection. J Virol. 2020;95(2).

765 38. Gentsch JR, Pacitti AF. Effect of neuraminidase treatment of cells and effect of
766 soluble glycoproteins on type 3 reovirus attachment to murine L cells. J Virol.
767 1985;56(2):356-64.

768 39. Avula K, Singh B, Kumar PV, Syed GH. Role of Lipid Transfer Proteins (LTPs) in
769 the Viral Life Cycle. Frontiers in microbiology. 2021;12:673509.

770 40. Lai CM, Mainou BA, Kim KS, Dermody TS. Directional release of reovirus from
771 the apical surface of polarized endothelial cells. mBio. 2013;4(2):e00049-13.

772 41. Fu J, Li L, Huo D, Zhi S, Yang R, Yang B, et al. Astrocyte-Derived TGFβ1
773 Facilitates Blood-Brain Barrier Function via Non-Canonical Hedgehog Signaling in Brain
774 Microvascular Endothelial Cells. Brain Sci. 2021;11(1).

775 42. Borsa J, Copps TP, Sargent MD, Long DG, Chapman JD. New intermediate
776 subviral particles in the in vitro uncoating of reovirus virions by chymotrypsin. J Virol.
777 1973;11(4):552-64.

778 43. Parker JS, Broering TJ, Kim J, Higgins DE, Nibert ML. Reovirus core protein m2
779 determines the filamentous morphology of viral inclusion bodies by interacting with and
780 stabilizing microtubules. J Virol. 2002;76(9):4483-96.

781 44. Aravamudhan P, Raghunathan K, Konopka-Anstadt J, Pathak A, Sutherland DM,
782 Carter BD, et al. Reovirus uses macropinocytosis-mediated entry and fast axonal
783 transport to infect neurons. PLoS Pathog. 2020;16(2):e1008380.

45. Elrick MJ, Yu T, Chung C, Lieberman AP. Impaired proteolysis underlies autophagic dysfunction in Niemann-Pick type C disease. Human molecular genetics. 2012;21(22):4876-87.

46. Carette JE, Raaben M, Wong AC, Herbert AS, Obernosterer G, Mulherkar N, et al. Ebola virus entry requires the cholesterol transporter Niemann-Pick C1. Nature. 2011;477(7364):340-3.

47. Miller EH, Obernosterer G, Raaben M, Herbert AS, Deffieu MS, Krishnan A, et al. Ebola virus entry requires the host-programmed recognition of an intracellular receptor. EMBO J. 2012;31(8):1947-60.

48. Rosenbaum AI, Zhang G, Warren JD, Maxfield FR. Endocytosis of beta-cyclodextrins is responsible for cholesterol reduction in Niemann-Pick type C mutant cells. Proc Natl Acad Sci U S A. 2010;107(12):5477-82.

49. Peake KB, Vance JE. Normalization of cholesterol homeostasis by 2-hydroxypropyl-β-cyclodextrin in neurons and glia from Niemann-Pick C1 (NPC1)-deficient mice. J Biol Chem. 2012;287(12):9290-8.

50. Liu B, Turley SD, Burns DK, Miller AM, Repa JJ, Dietschy JM. Reversal of defective lysosomal transport in NPC disease ameliorates liver dysfunction and neurodegeneration in the npc1-/- mouse. Proc Natl Acad Sci U S A. 2009;106(7):2377-82.

51. Ory DS, Ottinger EA, Farhat NY, King KA, Jiang X, Weissfeld L, et al. Intrathecal 2-hydroxypropyl-β-cyclodextrin decreases neurological disease progression in Niemann-Pick disease, type C1: a non-randomised, open-label, phase 1-2 trial. Lancet. 2017;390(10104):1758-68.

52. Poh MK, Shui G, Xie X, Shi PY, Wenk MR, Gu F. U18666A, an intra-cellular cholesterol transport inhibitor, inhibits dengue virus entry and replication. Antiviral research. 2012;93(1):191-8.

53. Cuesta-Geijo M, Chiappi M, Galindo I, Barrado-Gil L, Muñoz-Moreno R, Carrascosa JL, et al. Cholesterol Flux Is Required for Endosomal Progression of African Swine Fever Virions during the Initial Establishment of Infection. J Virol. 2016;90(3):1534-43.

54. Elgner F, Ren H, Medvedev R, Ploen D, Himmelsbach K, Boller K, et al. The Intracellular Cholesterol Transport Inhibitor U18666A Inhibits the Exosome-Dependent Release of Mature Hepatitis C Virus. J Virol. 2016;90(24):11181-96.

55. Yin X, Ambardekar C, Lu Y, Feng Z. Distinct Entry Mechanisms for Nonenveloped and Quasi-Enveloped Hepatitis E Viruses. J Virol. 2016;90(8):4232-42.

56. Rivera-Serrano EE, González-López O, Das A, Lemon SM. Cellular entry and uncoating of naked and quasi-enveloped human hepatoviruses. eLife. 2019;8.

57. Sobo K, Le Blanc I, Luyet PP, Fivaz M, Ferguson C, Parton RG, et al. Late endosomal cholesterol accumulation leads to impaired intra-endosomal trafficking. PloS one. 2007;2(9):e851.

58. Vanier MT. Niemann-Pick disease type C. Orphanet J Rare Dis. 2010;5:16.

825 59. Koller D, Lohner K. The role of spontaneous lipid curvature in the interaction of
826 interfacially active peptides with membranes. Biochimica et biophysica acta.
827 2014;1838(9):2250-9.

828 60. Maier O, Galan DL, Wodrich H, Wiethoff CM. An N-terminal domain of
829 adenovirus protein VI fragments membranes by inducing positive membrane curvature.
830 Virology. 2010;402(1):11-9.

831 61. Guo X, Steinkühler J, Marin M, Li X, Lu W, Dimova R, et al. Interferon-Induced
832 Transmembrane Protein 3 Blocks Fusion of Diverse Enveloped Viruses by Altering
833 Mechanical Properties of Cell Membranes. ACS Nano. 2021;15(5):8155-70.

834 62. Anafu AA, Bowen CH, Chin CR, Brass AL, Holm GH. Interferon-inducible
835 transmembrane protein 3 (IFITM3) restricts reovirus cell entry. J Biol Chem.
836 2013;288(24):17261-71.

837 63. Moyer CL, Wiethoff CM, Maier O, Smith JG, Nemerow GR. Functional genetic
838 and biophysical analyses of membrane disruption by human adenovirus. J Virol.
839 2011;85(6):2631-41.

840 64. Patel A, Mohl BP, Roy P. Entry of Bluetongue Virus Capsid Requires the Late
841 Endosome-specific Lipid Lysobisphosphatidic Acid. J Biol Chem. 2016;291(23):12408-
842 19.

843 65. Silva-Ayala D, López T, Gutiérrez M, Perrimon N, López S, Arias CF. Genome-
844 wide RNAi screen reveals a role for the ESCRT complex in rotavirus cell entry. Proc
845 Natl Acad Sci U S A. 2013;110(25):10270-5.

846 66. Snyder A, Abad A, Danthi, P. A CRISPR-Cas9 screen reveals a role for WD
847 repeat-containing protein (WDR81) in the entry of late penetrating viruses.
848 2021 https://biorxiv.org/cgi/content/short/2021.09.26.461887v1

849 67. Liu K, Jian Y, Sun X, Yang C, Gao Z, Zhang Z, et al. Negative regulation of
850 phosphatidylinositol 3-phosphate levels in early-to-late endosome conversion. J Cell
851 Biol. 2016;212(2):181-98.

852 68. Wheeler S, Schmid R, Sillence DJ. Lipid⁻Protein Interactions in Niemann⁻Pick
853 Type C Disease: Insights from Molecular Modeling. Int J Mol Sci. 2019;20(3).

854 69. Rentero C, Blanco-Munoz P, Meneses-Salas E, Grewal T, Enrich C. Annexins-
855 coordinators of cholesterol homeostasis in endocytic pathways. Int J Mol Sci.
856 2018;19(5):E1444.

857 70. de Diego I, Schwartz F, Siegfried H, Dauterstedt P, Heeren J, Beisiegel U, et al.
858 Cholesterol modulates the membrane binding and intracellular distribution of annexin 6.
859 J Biol Chem. 2002;277(35):32187-94.

860 71. Mayran N, Parton RG, Gruenberg J. Annexin II regulates multivesicular
861 endosome biogenesis in the degradation pathway of animal cells. EMBO J.
862 2003;22(13):3242-53.

863 72. Hirsch AJ. The use of RNAi-based screens to identify host proteins involved in
864 viral replication. Future Microbiol. 2010;5(2):303-11.

865 73. Puschnik AS, Majzoub K, Ooi YS, Carette JE. A CRISPR toolbox to study virus-
866 host interactions. Nat Rev Microbiol. 2017;15(6):351-64.

867 74. Furlong DB, Nibert ML, Fields BN. Sigma 1 protein of mammalian reoviruses
868 extends from the surfaces of viral particles. J Virol. 1988;62(1):246-56.

869 75. Virgin HW, Bassel-Duby R, Fields BN, Tyler KL. Antibody protects against lethal
870 infection with the neurally spreading reovirus type 3 (Dearing). J Virol.
871 1988;62(12):4594-604.

872 76. Smith RE, Zweerink HJ, Joklik WK. Polypeptide components of virions, top
873 component and cores of reovirus type 3. Virology. 1969;39(4):791-810.

874 77. Fecek RJ, Busch R, Lin H, Pal K, Cunningham CA, Cuff CF. Production of Alexa
875 Fluor 488-labeled reovirus and characterization of target cell binding, competence, and
876 immunogenicity of labeled virions. Journal of immunological methods. 2006;314(1-
877 2):30-7.

878 78. Wetzel JD, Chappell JD, Fogo AB, Dermody TS. Efficiency of viral entry
879 determines the capacity of murine erythroleukemia cells to support persistent infections
880 by mammalian reoviruses. J Virol. 1997;71(1):299-306.

881 79. Chandran K, Walker SB, Chen Y, Contreras CM, Schiff LA, Baker TS, et al. In
882 vitro recoating of reovirus cores with baculovirus-expressed outer-capsid proteins m1
883 and s3. J Virol. 1999;73(5):3941-50.

884 80. Orchard RC, Wilen CB, Doench JG, Baldridge MT, McCune BT, Lee YC, et al.
885 Discovery of a proteinaceous cellular receptor for a norovirus. Science.
886 2016;353(6302):933-6.

887 81. Doench JG, Fusi N, Sullender M, Hegde M, Vaimberg EW, Donovan KF, et al.
888 Optimized sgRNA design to maximize activity and minimize off-target effects of
889 CRISPR-Cas9. Nat Biotechnol. 2016;34(2):184-91.

890 82. Spence JS, Krause TB, Mittler E, Jangra RK, Chandran K. Direct visualization of
891 ebola virus fusion triggering in the endocytic pathway. mBio. 2016;7(1):e01857-15.

892 83. Dehairs J, Talebi A, Cherifi Y, Swinnen JV. CRISP-ID: decoding CRISPR
893 mediated indels by Sanger sequencing. Sci Rep. 2016;6:28973.

894 84. Olivio-Marin JC. Extraction of spots in biological images using multi-scale
895 products. Pattern Recognition. 2002;35(9):1989-96.

896

897 **FIGURE LEGENDS**

898

899 **FIG 1** CRISPR and siRNA screens identify NPC1 as a cellular factor required for
900 reovirus infection. (A) The top 20 candidates from the CRISPR screen using reovirus
901 strains T1L and T3D are ranked by their STAR scores. Heat map indicates STAR
902 values. (B) Genes from the siRNA screen using reovirus strain T3SA+ common to the
903 CRISPR screen using T1L and T3D, excluding ribosomal genes. Heat map indicates z-
904 score values. (C) Venn diagram of genes from the CRISPR screens using T1L and T3D
905 and the siRNA screen using T3SA+. (D) Molecular function pathways using Gene
906 Ontology to analyze genes from the CRISPR screen common to T1L and T3D. (E)
907 KEGG pathways identified for the CRISPR screen using T1L (red) and T3D (blue) and
908 siRNA screen using T3SA+ (light blue).

909

910 **FIG 2** Viral infectivity and titers following adsorption by reovirus virions and ISVPs. (A,
911 B) WT, KO, and KO+ HBMECs were adsorbed with reovirus (A) virions or (B) ISVPs at
912 MOIs of 10,000 or 100 particles/cell, respectively, and fixed at 18 h post-adsorption.
913 The percentage of infected cells was determined by enumerating reovirus-infected cells
914 following immunostaining with a reovirus-specific antiserum. (C-F) WT, KO, and KO+
915 cells were adsorbed with reovirus (C, E) virions at an MOI of 1 PFU/cell or (D, F) ISVPs
916 at an MOI of 5 particles/cell. Viral titers in cell-culture supernatants and lysates were
917 determined by plaque assay at 0, 24, and 48 h post-adsorption. The results are
918 presented as the mean of three independent experiments. Error bars indicated standard
919 deviation. *, $P < 0.05$; **, $P < 0.01$; ***, $P < 0.001$; ****, $P < 0.0001$, as determined by t-
920 test.

921

922 **FIG 3** Binding, internalization, and uncoating are not disrupted by cholesterol
923 accumulation in NPC1 KO HBMECs. (A) WT, KO, and KO+ HBMECs were adsorbed
924 with Alexa 647 labeled-reovirus virions at an MOI of 10,000 particles/cell at 4°C for 1 h,
925 fixed with 1% PFA, and analyzed for virus binding using flow cytometry. The results are
926 presented as mean virus binding as determined by mean fluorescence intensity (MFI) of
927 three independent experiments. Error bars indicated standard deviation. (B) WT, KO,
928 and KO+ HBMECs were adsorbed with Alexa 647 labeled-reovirus virions at an MOI of
929 10,000 particles/cell at 4°C for 45 min and imaged using high magnification live-cell
930 imaging, with images captured every ~ 25 seconds. Representative micrographs from
931 videos at the indicated intervals are shown. Scale bars, 10 μm. (C) WT, KO, and KO+
932 HBMECs were adsorbed with reovirus virions at an MOI of 10,000 particles/cell at 4°C
933 for 1 h and lysed at the intervals post-adsorption shown. Cell lysates were subjected to
934 electrophoresis and immunoblotting using a reovirus-specific polyclonal rabbit
935 antiserum. The results are presented as the mean ratio of the δ and μ1C bands from
936 three independent experiments. Error bars indicate standard deviation. Differences are
937 not significant, as determined by two-tailed unpaired t-test.
938
939 **FIG 4** Cytosolic entry of reovirus cores. (A) WT, KO, and KO+ HBMECs were adsorbed
940 with Alexa 647 labeled-reovirus virions at an MOI of 10,000 particles/cell at 37°C for 45
941 min and fixed with 4% PFA at 8 h post-adsorption. Cells were stained with DAPI, a CD-
942 63-specific antibody to label endosomes, and an antiserum specific for reovirus cores,
943 and imaged using confocal microscopy. Representative confocal micrographs are
944 shown. (B) Colocalization of reovirus, cores, and endosomes was analyzed using the
945 JaCoP plugin function from ImageJ. The results are presented as the mean
946 colocalization (quantified by Manders coefficient) of ~ 50 cells from three independent

947 experiments. Error bars indicate standard deviation. **, $P < 0.01$; ***, $P < 0.001$, as
948 determined by two-tailed unpaired t-test.
949
950 **FIG 5** Synthesis of nascent RNA is reduced in NPC1 KO HBMECs. WT, KO, and KO+
951 HBMECs were adsorbed with reovirus virions at an MOI of 1 PFU/cell at 37°C for 1 h,
952 lysed at the intervals post-adsorption shown, and assayed for positive-sense reovirus
953 s4 RNA by RT-qPCR. The results are presented as the mean number of copies of
954 reovirus s4 RNA by qPCR from two independent experiments. Error bars indicate
955 standard errors of the mean. **, $P < 0.01$; ***, $P < 0.001$, as determined by t-test.
956
957 **FIG 6** HβCD treatment restores reovirus infection of NPC1 KO HBMECs. WT, KO, and
958 KO+ HBMECs were pretreated with 1 mM HβCD or PBS for 24 h, adsorbed with
959 reovirus virions or ISVPs at MOIs of 10,000 or 100 particles/cell, respectively, and fixed
960 at 18 h post-adsorption. The percentage of infected cells was determined by
961 enumerating reovirus-infected cells following immunostaining with a reovirus-specific
962 antiserum. The results are presented as the mean of three independent experiments.
963 Error bars indicated standard deviation. ***, $P < 0.001$ as determined by two-tailed
964 unpaired t-test.
965
966 **SUPPLEMENTAL MATERIALS**
967 **FIGURES AND MOVIES**
968
969 **FIG S1** Effect on cholesterol distribution by disruption of NPC1 expression. (A, B)
970 Lysates of WT, KO, and KO+ HBMECs were subjected to electrophoresis and
971 immunoblotting using an NPC1 antiserum. GAPDH was used as loading control. A

972 representative immunoblot is shown. The results are presented as the mean of two
973 independent experiments. Error bars indicate standard deviation. Statistical analysis
974 was done by two-tailed unpaired t-test. (C) WT, KO, and KO+ HBMECs were stained
975 with filipin III to detect cholesterol distribution. Representative images are shown. Scale
976 bars, 10 μm. (D) WT, KO, and KO+ HBMECs were stained with filipin III and an anti-
977 CD63 antibody to detect the subcellular localization of cholesterol. Representative
978 images are shown. Scale bars, 10 μm.
979 **FIG S2** Viral infectivity following adsorption by T1L, T3D, and T3SA+ virions. (A, B) WT,
980 KO, and KO+ HBMECs were adsorbed with reovirus virions at MOIs of 10,000
981 particles/cell, and fixed at 18 h post-adsorption. The percentage of infected cells was
982 determined by enumerating reovirus-infected cells following immunostaining with a
983 reovirus-specific antiserum. Error bars indicated standard deviation. **, $P < 0.01$; ***, P
984 < 0.001, as determine by 2 way ANOVA, Tukey's multiple comparisons test.
985 **FIG S3** HβCD treatment restores cholesterol efflux in KO cells. (A) WT, KO, and KO+
986 HBMECs were treated with HβCD at the concentrations shown for 48 h and assessed
987 for viability using the Presto blue cell viability reagent. The results are presented as the
988 mean cell viability of three independent experiments. Error bars indicated standard
989 deviation. **, $P < 0.01$; ***, $P < 0.001$; ****, $P < 0.0001$, as determined by two-way
990 ANOVA. (B, C) Cells were treated with 1 mM HβCD or PBS (mock) for 48 h, fixed with
991 4% PFA, stained with filipin III, and imaged using confocal microscopy. (B) The results
992 are presented as the mean filipin III staining (quantified by MFI) of ~ 50 cells from three
993 independent experiments. Error bars indicate the minimum and the maximum values. *,
994 $P < 0.05$; ****, $P < 0.0001$, as determined by two-tailed unpaired t-test. (C)
995 Representative images of cholesterol distribution in HβCD-treated and mock-treated
996 cells are shown. Scale bars, 10 μm.

997

998 **VIDEO 1, 2, and 3** High-magnification, live-cell microscopy of fluorescent reovirus virion
999 transport in WT, KO, and KO+ HBMECs. (1) WT, (2) KO, and (3) KO+ cells were
1000 adsorbed with Alexa 647-labeled reovirus virions at an MOI of 10,000 particles/cell at
1001 4ºC for 45 min. Fluorescence and brightfield images were captured every ~ 25 seconds
1002 for 36 min.

1003

1004 **VIDEO 4, 5, and 6** Tracking of fluorescent reovirus virions recruited to a perinuclear
1005 region following entry. Trajectories of reovirus virions during internalization into WT, KO,
1006 and KO+ HBMECs from videos 1, 2, and 3 were tracked with the spot-tracking plugin
1007 function of Icy-Bioimage analysis software (84). Cell contour was defined as a region of
1008 interest (ROI), and ~ 7 pixels/spot were monitored. The colored bar represents the
1009 trajectory depending on time, in which each color (from yellow to red) corresponds to an
1010 interval of ~ 7.5 min in the time-lapse videos. Scale bars, 10 μm.

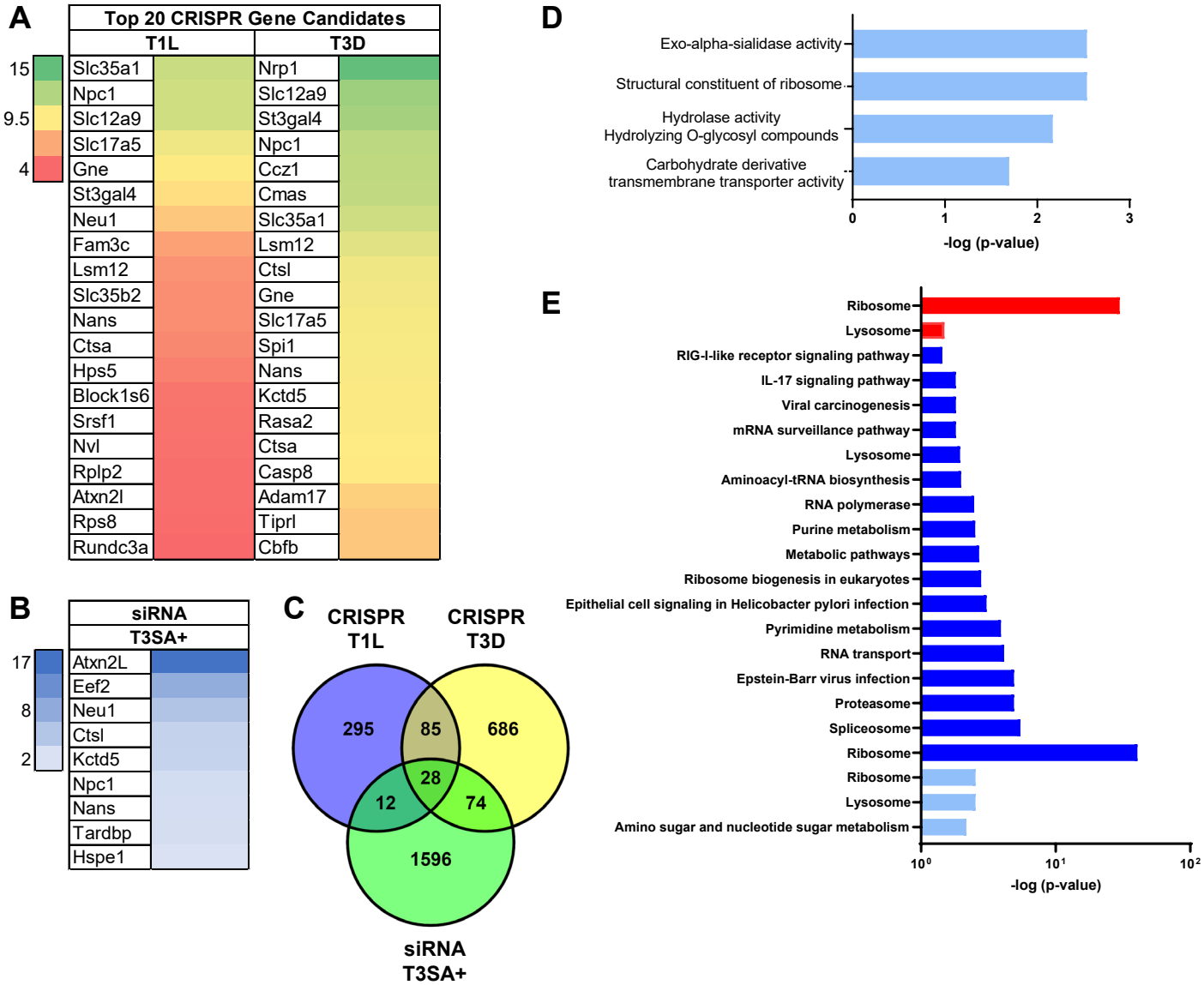

FIG 1 CRISPR and siRNA screens identify NPC1 as a cellular factor required for reovirus infection. (A) The top 20 candidates from the CRISPR screen using reovirus strains T1L and T3D are ranked by their STAR scores. Heat map indicates STAR values. (B) Genes from the siRNA screen using reovirus strain T3SA+ common to the CRISPR screen using T1L and T3D, excluding ribosomal genes. Heat map indicates z-score values. (C) Venn diagram of genes from the CRISPR screens using T1L and T3D and the siRNA screen using T3SA+. (D) Molecular function pathways using Gene Ontology to analyze genes from the CRISPR screen common to T1L and T3D. (E) KEGG pathways identified for the CRISPR screen using T1L (red) and T3D (blue) and siRNA screen using T3SA+ (light blue).

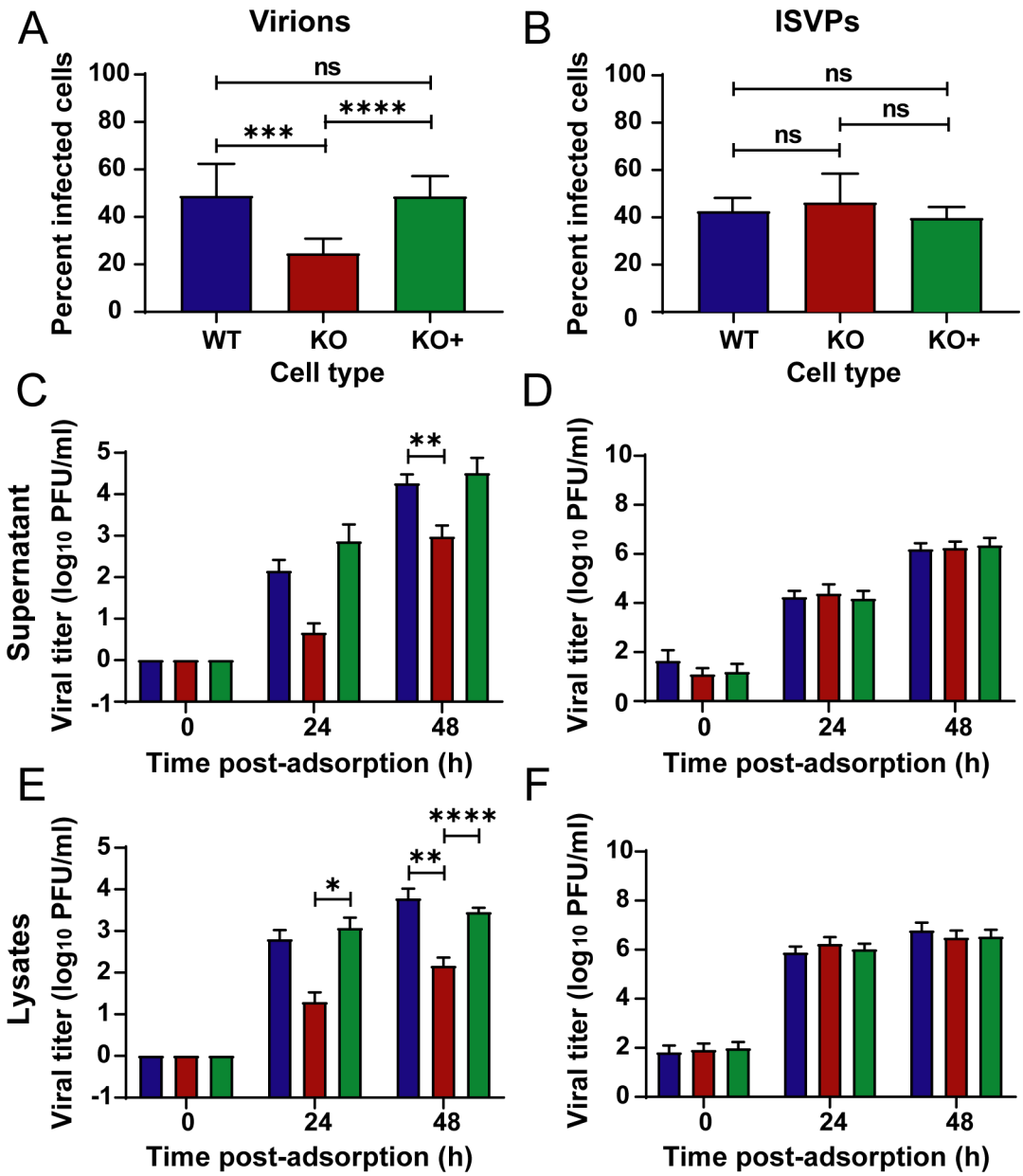

FIG 2 Viral infectivity and titers following adsorption by reovirus virions and ISVPs. (A, B) WT, KO, and KO+ HBMECs were adsorbed with reovirus (A) virions or (B) ISVPs at MOIs of 10,000 or 100 particles/cell, respectively, and fixed at 18 h post-adsorption. The percentage of infected cells was determined by enumerating reovirus-infected cells following immunostaining with a reovirus-specific antiserum. (C-F) WT, KO, and KO+ cells were adsorbed with reovirus (C, E) virions at an MOI of 1 PFU/cell or (D, F) ISVPs at an MOI of 5 particles/cell. Viral titers in cell-culture supernatants and lysates were determined by plaque assay at 0, 24, and 48 h post-adsorption. The results are presented as the mean of three independent experiments. Error bars indicated standard deviation. *, $P < 0.05$; **, $P < 0.01$; ***, $P < 0.001$; ****, $P < 0.0001$, as determined by t-test.

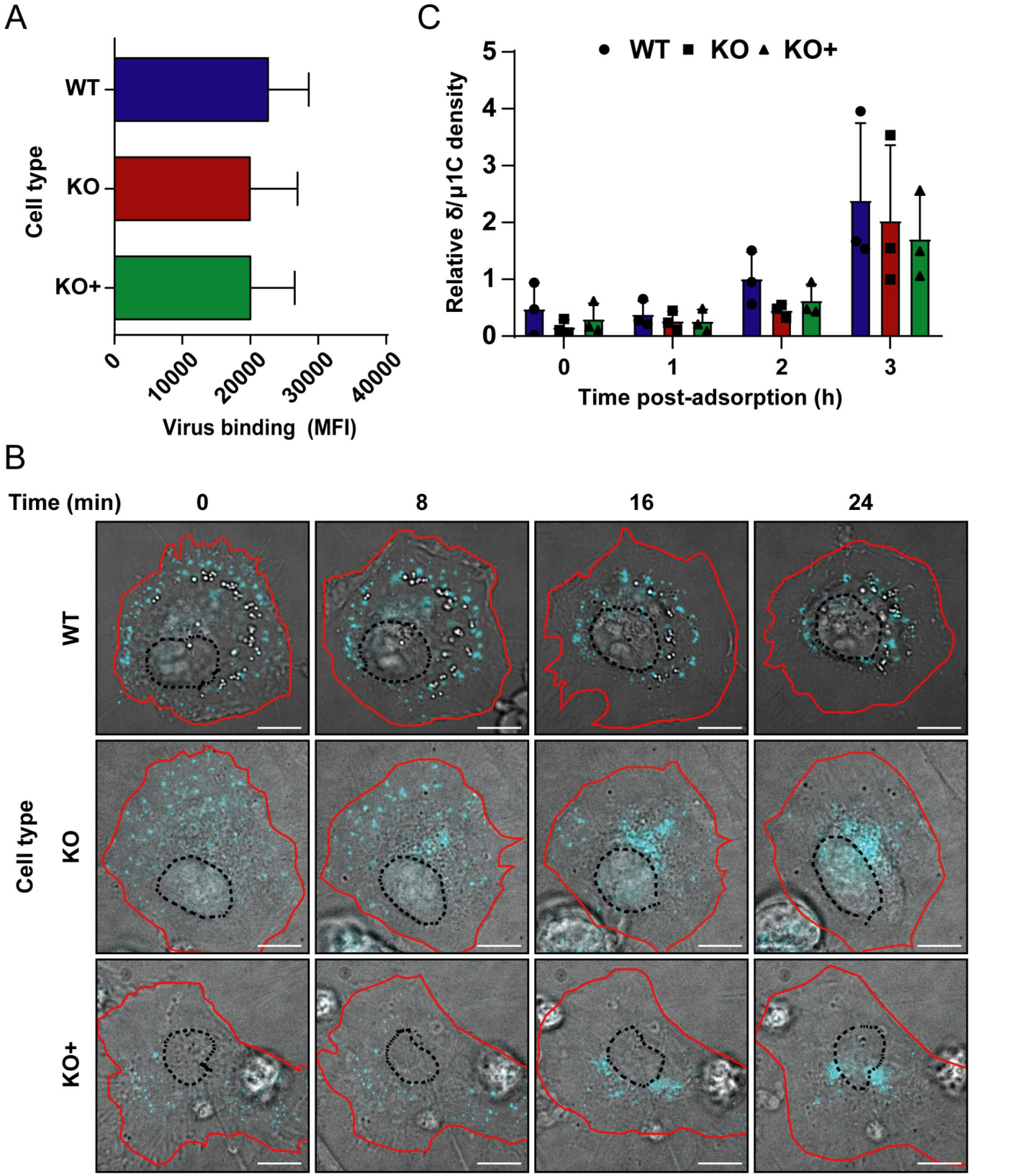

FIG 3 Binding, internalization, and uncoating are not disrupted by cholesterol accumulation in NPC1 KO HBMECs. (A) WT, KO, and KO+ HBMECs were adsorbed with Alexa 647 labeled-reovirus virions at an MOI of 10,000 particles/cell at 4°C for 1 h, fixed with 1% PFA, and analyzed for virus binding using flow cytometry. The results are presented as mean virus binding as determined by mean fluorescence intensity (MFI) of three independent experiments. Error bars indicated standard deviation. (B) WT, KO, and KO+ HBMECs were adsorbed with Alexa 647 labeled-reovirus virions at an MOI of 10,000 particles/cell at 4°C for 45 min and imaged using high magnification live-cell imaging, with images captured every ~ 25 seconds. Representative micrographs from videos at the indicated intervals are shown. Scale bars, 10 μm. (C) WT, KO, and KO+ HBMECs were adsorbed with reovirus virions at an MOI of 10,000 particles/cell at 4°C for 1 h and lysed at the intervals post-adsorption shown. Cell lysates were subjected to electrophoresis and immunoblotting using a reovirus-specific polyclonal rabbit antiserum. The results are presented as the mean ratio of the δ and μ1C bands from three independent experiments. Error bars indicate standard deviation. Differences are not significant, as determined by two-tailed unpaired t-test.

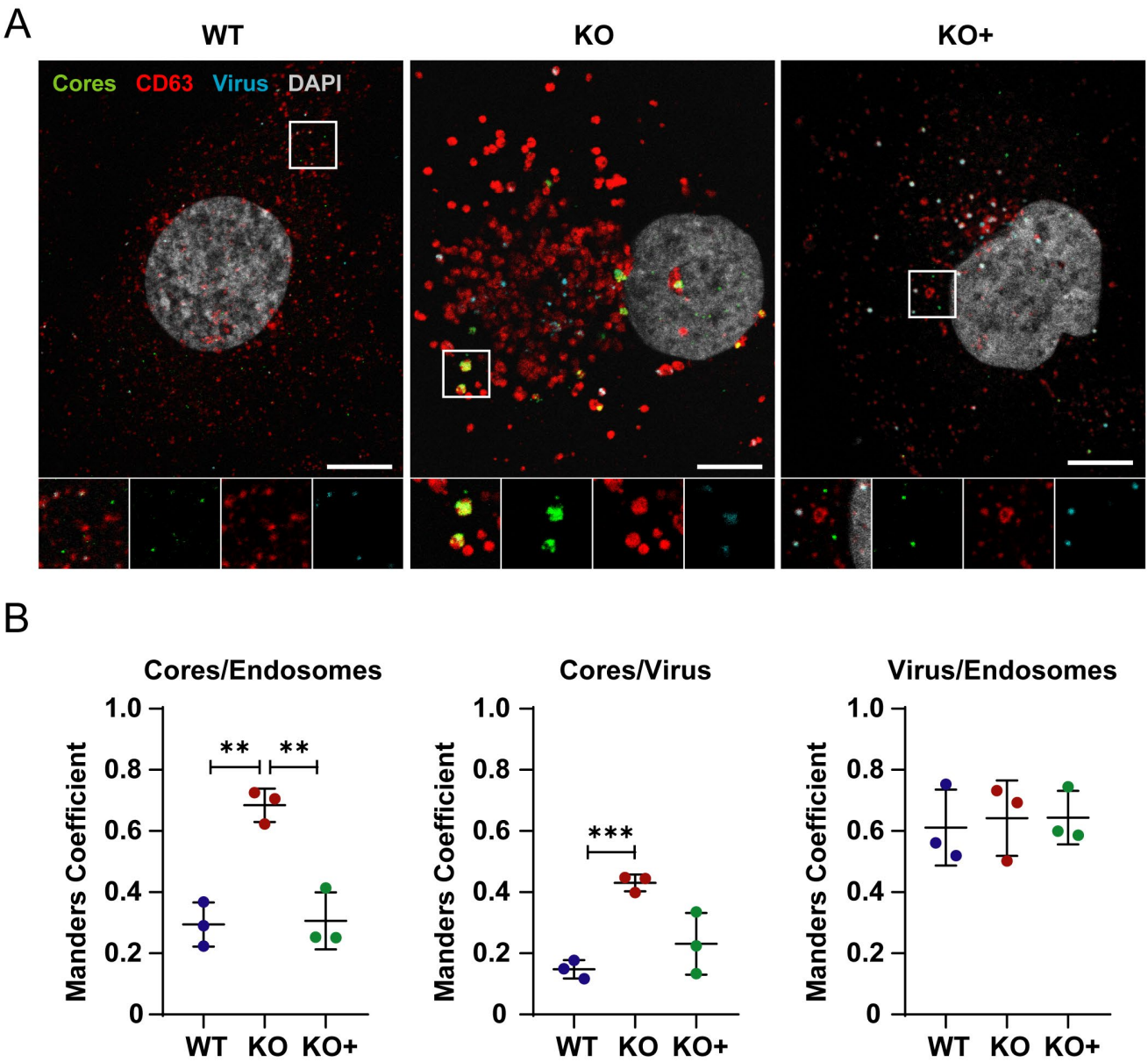

FIG 4 Cytosolic entry of reovirus cores. (A) WT, KO, and KO+ HBMECs were adsorbed with Alexa 647 labeled-reovirus virions at an MOI of 10,000 particles/cell at 37°C for 45 min and fixed with 4% PFA at 8 h post-adsorption. Cells were stained with DAPI, a CD-63-specific antibody to label endosomes, and an antiserum specific for reovirus cores, and imaged using confocal microscopy. Representative confocal micrographs are shown. (B) Colocalization of reovirus, cores, and endosomes was analyzed using the JaCoP plugin function from ImageJ. The results are presented as the mean colocalization (quantified by Manders coefficient) of ~ 50 cells from three independent experiments. Error bars indicate standard deviation. **, $P < 0.01$; ***, $P < 0.001$, as determined by two-tailed unpaired t-test.

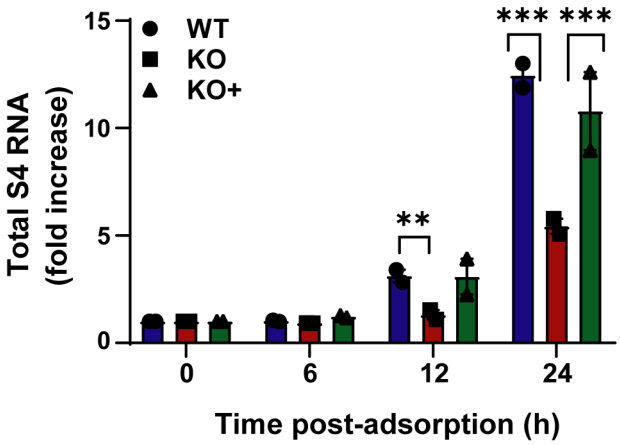

FIG 5 Synthesis of nascent RNA is reduced in NPC1 KO HBMECs. WT, KO, and KO+ HBMECs were adsorbed with reovirus virions at an MOI of 1 PFU/cell at 37°C for 1 h, lysed at the intervals post-adsorption shown, and assayed for positive-sense reovirus s4 RNA by RT-qPCR. The results are presented as the mean number of copies of reovirus s4 RNA by qPCR from two independent experiments. Error bars indicate standard errors of the mean. **, $P < 0.01$; ***, $P < 0.001$, as determined by t-test.

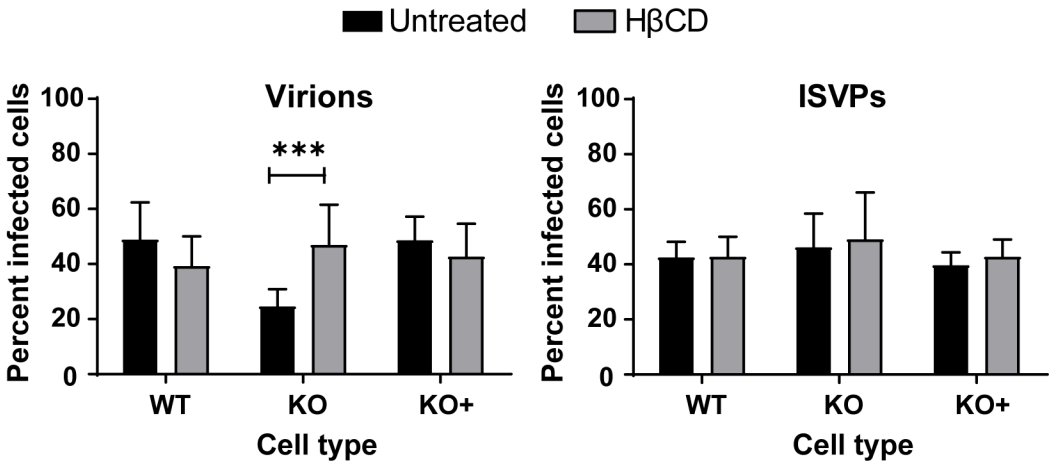

FIG 6 HβCD treatment restores reovirus infection of NPC1 KO HBMECs. WT, KO, and KO+ HBMECs were pretreated with 1 mM HβCD or PBS for 24 h, adsorbed with reovirus virions or ISVPs at MOIs of 10,000 or 100 particles/cell, respectively, and fixed at 18 h post-adsorption. The percentage of infected cells was determined by enumerating reovirus-infected cells following immunostaining with a reovirus-specific antiserum. The results are presented as the mean of three independent experiments. Error bars indicated standard deviation. ***, $P < 0.001$ as determined by two-tailed unpaired t-test.